COMPOSITION AND STRUCTURE OF THE SOUTH POLE-AITKEN BASIN IMPACT MELT SHEET. Debra M. Hurwitz[1,2] and David A. Kring[1,2]; [1]Center for Lunar Science and Exploration, Lunar and Planetary Institute, 3600 Bay Area Blvd., Houston, TX, 77058, [2]NASA Lunar Science Institute (hurwitz@lpi.usra.edu)

Introduction: The South Pole-Aitken (SPA) basin represents a unique lunar terrane with distinctive chemical signatures (e.g., [1-3]). Analyses of Clementine UVVIS spectra (e.g., [1]) indicate high concentrations of mafic rocks within the central region of SPA, including norite with low-Ca pyroxene as the dominant mafic mineral and gabbro and basalt with high-Ca pyroxene as the dominant mafic mineral. Additionally, enhancements in FeO and TiO_2 relative to adjacent highland terranes (e.g., [2,3]) are interpreted to indicate the presence of a mixture of mantle and lower crustal materials exposed in the interior of the SPA basin. These lithologies may represent either the remnants of melt generated during the impact process or a different type of lower crustal material than previously sampled [2]. The current study investigates an impact melt origin for the material within the SPA basin in an effort to better understand how large volumes of melt evolved on the Moon.

Methods: The primary question addressed in this study is: Can impact melt differentiation account for the noritic and gabbroic lithologies observed within the central SPA basin? To address this question, we must estimate the bulk composition of the impact melt sheet, a composition that is influenced by the target lithologies present prior to impact and by the structure of the lunar interior during and after basin formation. Recent analyses of GRAIL gravity data [4,5] indicate the farside lunar crust outside the SPA basin currently has an average thickness of ~45 km, and recent analyses of Apollo seismic data suggest that the lunar core has a radius of ~480 km [6], leaving a mantle with a depth of 1212 km to account for a total lunar radius of 1737 km. This distribution is assumed to represent pre-SPA lunar structure and is illustrated in Fig. 1 with the zones of material that were vaporized, melted, and excavated upon impact ([7], Potter, R. W. K., pers. comm., 2012). Excavation to a depth of ~100 km removed all of the crust and a portion of the upper mantle within the transient crater (depth, 390 km; diam, 820 km, [7]). The melt zones shown indicate the depths of 100% melting (250 km) and incomplete (50-100%) melting (400 km, Potter, R. W. K., pers. comm., 2012). These melt regions consumed portions of Lunar Magma Ocean (LMO) cumulates to produce the SPA melt sheet. After the impact (not shown), the melt was concentrated in a melt sheet with a diameter of ~200 km and depth of ~50 km [7]. This melt sheet might include melted cumulates either from the 100% melt zone alone or from a mixture of material from both melt zones shown.

The type of LMO material melted by the impact depends on the initial bulk composition of the Moon and how the LMO solidified. Three cases were considered based on recent experimental results of LMO

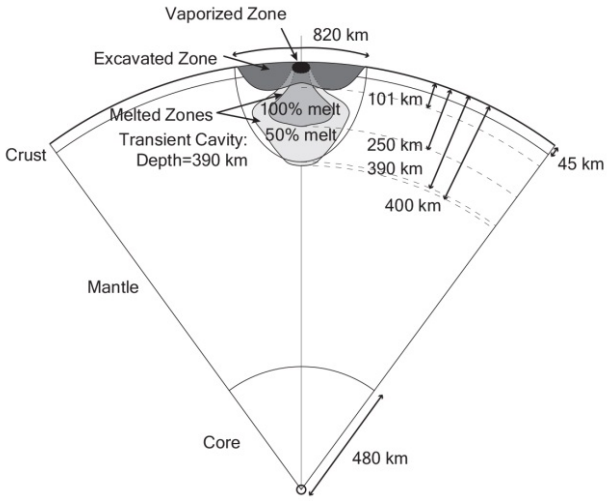

Figure 1: Zones within the Moon that were vaporized, melted, and excavated by the SPA basin impact event that produced a final basin diameter of ~2200 km. Details of the geometries shown are in the text.

crystallization. These include an initial bulk lunar composition equivalent to Lunar Primitive Upper Mantle (LPUM, [8]) and to Taylor Whole Moon (TWM, [9]) oxide concentrations, with 50 vol% LMO solidification by equilibrium crystallization followed by 50 vol% LMO solidification by fractional crystallization ([10], hereafter Elardo LPUM and Elardo TWM), and an initial composition equivalent to TWM with 100% LMO solidification by fractional crystallization ([11,12], hereafter Rapp TWM). Experimental results have not yet been completed to simulate fully crystallized LMO scenarios, so we use PETROLOG [13] to calculate the compositions of the shallow portions of each LMO case. PETROLOG was chosen for this study because it was most appropriate for shallow lunar conditions, where the melt has an oxygen fugacity of IW–1 [14] and no longer crystallizes olivine. Additionally, PETROLOG faithfully reproduces experimental results at lower pressures (e.g., Elardo TWM, 1 GPa, ~200 km depth).

For each of the three initial bulk lunar compositions and LMO systems described above, three melt sheet scenarios were considered. In one case, the melt sheet was produced from the upper 250 km of the LMO (i.e., the 100% melt zone of [7]). In the second case, the melt sheet contained 28% of material from the 100% melt zone of Fig. 1 and 72% of material from the incomplete melt zone (the relative weights are approximations of the differences in melt zone volumes). These melt sheet scenarios assume that the SPA impact occurred before LMO overturn. In a third case, the melt sheet was produced after LMO overturn brought cumulates from a depth of ~420 km to the shallow lunar subsurface. This melt composition was simulated by adding the cumulates at depth (olivine with a

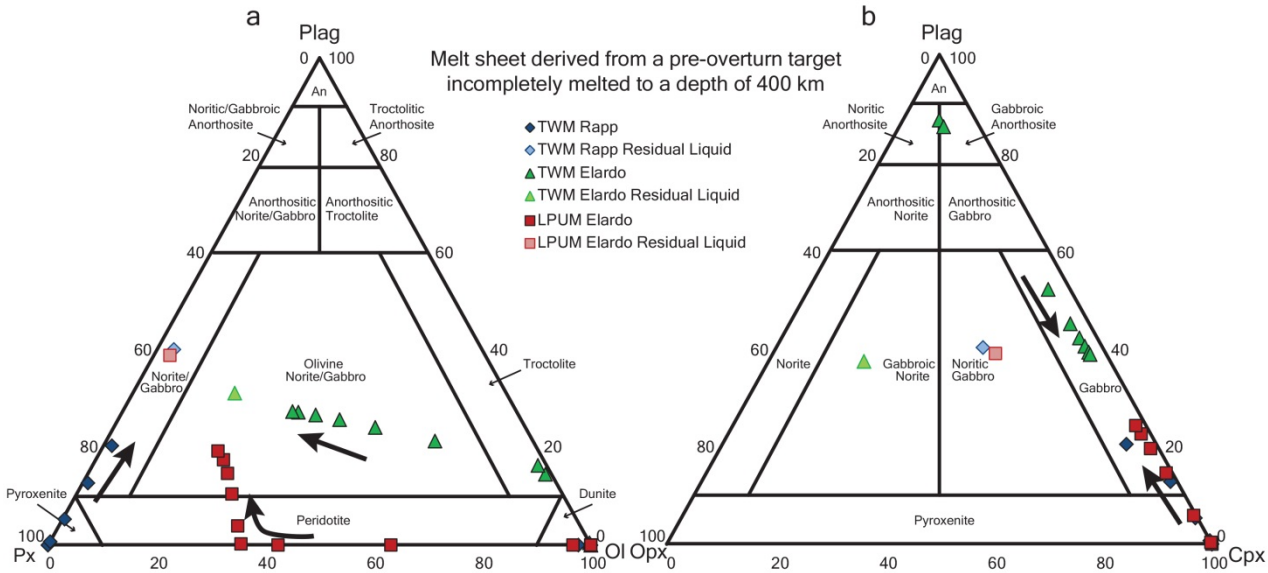

Figure 2: Compositions of cumulates from SPA impact melt sheet in (a) a Plag-Px-Ol ternary and (b) a Plag-Opx-Cpx ternary, with results shown for a pre-overturn LMO target incompletely melted to a depth of 400 km. The compositions of all melt sheet scenarios shown evolve towards gabbroic and/or noritic materials.

Mg# of ~89, [10]) to the material from the 100% melt zone in a 1:1 ratio. In all cases, the composition of anorthositic crust (e.g., [15]) was subtracted to account for excavation of the crust within the transient crater.

These nine initial melt compositions were used as inputs into PETROLOG to simulate solidification of the melt sheet, and results are shown in ternary form (Fig. 2) and a representative cross section (Fig. 3) that shows the vertical structure of the central melt sheet.

Results: The evolution of the melt sheet (50 km depth) for the Elardo TWM scenario is illustrated with green triangles in Fig. 2 as it solidified from a pre-overturn LMO target incompletely melted to a depth of 400 km. Figure 2 also includes similar results from cases that began with the initial bulk Moon compositions of Rapp TWM (blue diamonds) and Elardo LPUM (red squares) for comparison. In all three cases shown, the compositions of the melt sheets evolve towards gabbroic and/or noritic materials. The effective cross section of a solidified impact melt sheet assuming the Elardo TWM pre-impact scenario is shown in Fig. 3. Dunite initially crystallized from the melt sheet to a depth of 42 km, at which depth troctolite began to form. At a depth of 39 km, high-Ca pyroxene began to crystallize, resulting in the formation of an olivine gabbro cumulate. The generation of this lithology was predicted to continue until the model halted at a depth of 11 km, leaving behind a remnant melt of olivine gabbroic norite.

Figure 3: Cross section of a melt sheet with a starting composition similar to a pre-overturn Elardo TWM LMO target melted to a depth of 400 km. The uppermost remnant melt composition is consistent with observations of gabbro and norite in the interior of the SPA basin. Depths were calculated using the P-z profile defined in [16].

Conclusions: Remotely observed surface compositions within the SPA basin may correspond to either the top of a quenched melt sheet, the upper remains of a differentiated melt sheet, lavas emplaced after melt sheet formation, or a combination of some or all of these scenarios. Results from this study suggest that the quenched melt sheet would have had a composition that is more ultramafic than observed, suggesting that this uppermost melt sheet layer is no longer at the surface. Results suggest instead that the noritic and gabbroic materials at the surface are remnants of a differentiated melt sheet with a mantle-dominated source and/or that these materials are eruptives from evolved portions of the differentiated melt sheet emplaced on top of any quenched surface.

Acknowledgements: We would like to thank J. Rapp, R. Potter, and Y. Sonzogni for extensive discussions that facilitated the development and execution of this work.

References: [1] Pieters, C.M. et al., 2001, JGR, 106, 28,001; [2] Lucey, P.G., et al., 1996, LPSC, 27, 783; [3] Jolliff, B.L., et al., 2000, JGR, 105, 4197; [4] Wieczorek, M.A., et al., 2012, Science, doi:10.1126/ science.1231530; [5] Zuber, M.T., et al., 2012, Science, doi: 10.1126/ science.1231507; [6] Weber, R.C., et al., 2011, Science, 331, 309; [7] Potter, R.W.K., et al., 2012, Icarus, 220, 730; [8] Longhi, J., 2006, Geochim. Cosmochim. Acta, 70, 5919; [9] Taylor, S.R., 1982, Planetary Science: A Lunar Perspective, LPI, Houston, TX; [10] Elardo, S.M., et al., 2011, Geochim. Cosmochim. Acta, 75, 3024; [11] Rapp, J. and Draper, D.,2012, LPSC, 43, 2048; [12] Rapp, J. and Draper, D., 2013, LPSC, 44; [13] Danyushevsky, L.V., and P.Plechov, 2011, Geochem. Geophys. Geosyst., 12, Q07021, doi:10.1029/2011GC003516, 32 p; [14] Papike, J.J., et al., 1998, Rev. Mineral., 36, 234; [15] Korotev, R.L., et al., 2003, Geochim. Cosmochim. Acta, 67, 4895; [16] Elkins-Tanton, L.T., et al., 2011, EPSL, 304, 326.